Estimating Muscle Fibre Conduction Velocity in the Presence of Array Misalignment

Christopher Gilliam and Beth Jelfs
RMIT University, Melbourne, Australia
E-mail: {christopher.gilliam,beth.jelfs}@rmit.edu.au

***Abstract*—Surface electromyography (sEMG) has the potential to provide valuable information regarding the status and health of a muscle. In particular, recent developments in high density sEMG (HD-sEMG), which allow simultaneous recordings from a greater number of electrodes, enable the calculation of muscle attributes such as the conduction velocity of motor unit action potentials. However, as with standard recording montages, HD-sEMG requires careful placement of the electrodes to align with the direction of the muscle fibres, thus limiting practical applications. In this paper we demonstrate an algorithm for calculating muscle fibre conduction velocity which is independent of the alignment of the array. The algorithm automatically corrects for the misalignment of the array whilst estimating the conduction velocity using common local all-pass (CLAP) filters. Specifically, the misalignment is modelled as a rotation of the array relative to the fibre and this rotation is estimated by iteratively fitting the model to the output of the CLAP filters. We validate the proposed algorithm on simulated HD-sEMG data generated from a realistic biological model, demonstrating that the algorithm obtains an accurate estimate of the conduction velocity even when the array is misaligned.**

I. Introduction

Surface electromyography (sEMG) provides a measure of the electrical activity produced during muscle contractions. Due to its ease of use and non-invasive nature, sEMG has attracted attention in a number of different areas from rehabilitation and prosthetics to human computer interfaces [1]. Developments in sensor technologies, flexible electrodes and wireless devices have the potential to allow for small portable recording devices for sEMG. Such devices can be used in a greater range of recording scenarios allowing the monitoring of muscle activity to be taken out of a laboratory setting and into everyday life. Despite the many desirable properties of sEMG there are also limitations [2]. Recordings of sEMG are affected by the impedance between the skin and the electrode; are subject to noise and interference - both biological and external; and are impacted by the location of the recording site in relation to the muscle. Hence, a great deal of effort has gone not only into guidelines regarding the recording of sEMG [3] but also into developing techniques for the processing and identification of features of sEMG [1], [4].

The signals acquired via sEMG are superpositions of the activities of the motor units (MUs)[1] within the recording region of the electrode. As such, there is the potential to provide valuable information regarding the neurological control, health and status of the muscle [4]. One important muscle attribute which has the potential to inform on neurological diseases and can be measured using sEMG is the muscle fibre conduction velocity (MFCV) [5]. MFCV describes the speed at which MU action potentials (MUAPs) are propagating along the muscle fibre and also finds application in measuring muscle fatigue for sports or rehabilitation. A number of methods for estimating MFCV have been proposed [6], [7], [8], [9], [10], however, the problem is not straightforward and there are known difficulties surrounding measuring MFCV.

Estimation of MFCV often requires careful placement of the electrodes in terms of alignment with the fibres and location with respect to the innervation zone (IZ) and tendon regions. All of which can affect estimates of conduction velocity (CV) [11]. However, it is not only the recording set-up which can impact upon the estimate of the MFCV there are also a number of different physiological factors which affect measurements of the MFCV. During the course of a contraction changes in the CVs of individual motor units, as well as changes in recruitment and synchronization of MUs can also affect the overall MFCV. Hence, MFCV is time-varying in nature and requires an estimation method which can not only measure but also track changes in CV. However, many of the MFCV estimation methods only provide fixed CV estimates limiting their application.

High density sEMG (HD-sEMG) which uses 2D electrode arrays has been shown to reduce the sensitivity to electrode displacements [6] and provide accurate estimates of time-varying MFCV [9], [10]. However, the issue of alignment with the direction of the fibres remains. In [8] a method for estimating both MFCV and the fibre orientation with respect to the 2D electrode array was proposed. However, this method did not consider time-varying velocities and was reliant on tracking the propagation of individual MUAPs through the electrode array. Hence it was tested on simulations with only a small number of MUs (up to nine) and real data from very low level contractions (5% of maximum voluntary contraction). Again this limits practical application of the technique as typical muscle contractions involve stronger contractions and larger numbers of MUs.

In [12] we proposed a method for estimating MFCVs using local all-pass filters by posing the problem as estimating a common time-varying delay (TVD) from an ensemble of signals. The proposed common local all-pass (CLAP) algorithm was shown to be accurate in the presence of noise

[1] A motor unit comprises of a single motor neuron which innervates a group of muscle fibres

and insensitive to positioning of the array; thus, addressing limitations with previous time-varying estimators by providing a method to automatically identify the IZ. In this paper we propose an extension of the CLAP algorithm to allow accurate estimation of the MFCV irrespective of the the alignment of the electrode array with respect to the muscle fibres. The misalignment between the array and the muscle fibres is modelled as a rotation of the array. This rotation is then estimated by applying the CLAP algorithm both along the columns of the array and across the rows of the array to produce TVD vectors. The angle of rotation is obtained from the mean angle of the vectors and the process iterated to improve the estimation. Finally, the estimate of the MFCV is obtained by applying the CLAP algorithm along the columns of the rotation corrected array. We validate the proposed approach using a realistic biological model which allows us to control the position and alignment of the electrode array and the properties of the MUs which contribute to the simulated HD-sEMG.

II. Delay Estimation Framework

The problem of estimating MFCV can be formulated as estimating a TVD between signals obtained from spatially separated recording electrodes such that

$$\begin{aligned} g_1(t) &= f(t) + e_1(t) \\ g_2(t) &= f\big(t - \tau(t)\big) + e_2(t) \\ &\vdots \\ g_N(t) &= f\big(t - (N-1)\tau(t)\big) + e_N(t), \end{aligned} \tag{1}$$

where $g_n(t)$ is the signal recorded at the n^{th} electrode at time t, N is the number of electrodes, $f(t)$ is the signal of interest and $\tau(t)$ is the TVD common to all electrodes. The additive noises $e_n(t)$ are assumed to be i.i.d Gaussian processes. However, this model is based upon the assumption of a signal propagating in the same direction as the electrode array. If we consider a 2D array this assumption is only valid in the case of perfect alignment between the columns of the array and the muscle fibres as in Fig. 1a. If, in fact, there is misalignment between the electrode array and the muscle fibres as in Fig. 1b, the signals propagate at an angle θ to the array. Then the true delay becomes

$$\begin{aligned} \tau(t) =& \tau_{\text{col}}(t) + j\,\tau_{\text{row}}(t) \\ =& |\tau(t)|\,(\cos\theta + j\sin\theta) \end{aligned} \tag{2}$$

meaning the estimate of the delay along the columns is

$$\tau_{\text{col}}(t) = |\tau(t)|\cos\theta \tag{3}$$

which unless $\theta = 1$ results in an underestimate of $\tau(t)$ and hence an overestimate of the MFCV. Thus, for accurate estimation of the MFCV we require a method which takes into account not only calculation of the delay but also the angle of any misalignment between the electrode array and the muscle fibres. The method proposed in [12] accurately estimated the delay τ_{col} and here we extend this method to jointly estimate the delay whilst also correcting for the misalignment.

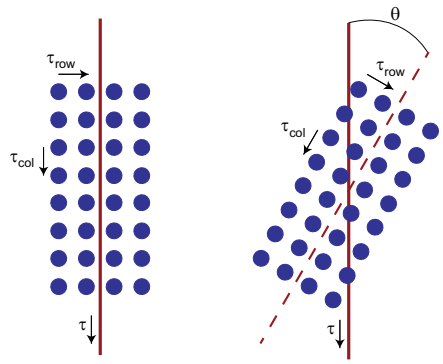

(a) Perfect Alignment (b) Misalignment

Fig. 1. Diagram showing the effect of electrode misalignment on the delay estimation. The solid red lines indicate the direction of the fibres and the dashed line the alignment of the array, the blue circles are the electrodes.

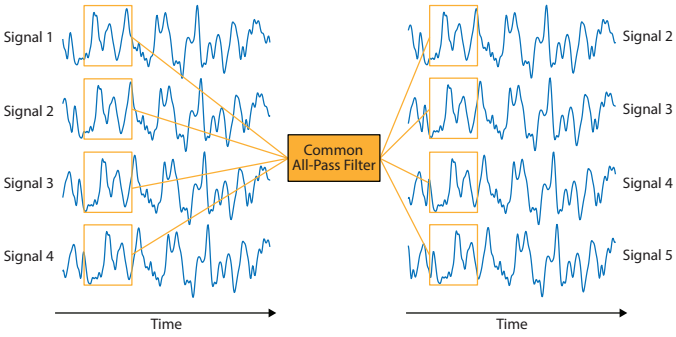

Fig. 2. Diagram illustrating the principle of the CLAP algorithm. Local regions on the left-hand side are related to corresponding locations on the right-hand side via a common all-pass filter.

A. Common Local All-Pass Filters

We first introduce the CLAP algorithm presented in [12] for estimating a TVD that is common across an ensemble of signals as described in (1). The algorithm originates from the local all-pass framework proposed in image registration [13] and has previously been applied to 3D MR images [14] and protein tracking in fluorescence microscopy images [15].

The central concept of the CLAP algorithm is that two sets of signals can be related, on a local level, using all-pass filters. This concept is illustrated in Fig. 2. The CLAP functions by assuming the common delay signal $\tau(t)$ is locally constant within the regions marked in yellow. Under this assumption, the constant delay is equivalent to filtering with an all-pass filter (this follows naturally from the Fourier shift theorem). Accordingly, within the local regions, the algorithm seeks to estimate an all-pass filter h, with a frequency response $H(\omega) = \mathrm{e}^{-j\tau\omega}$, as a proxy for determining the delay. An estimate of the delay is then extracted from the all-pass filter. This process is repeated for every sample to obtain an estimate of the common TVD signal.

In more detail, the filter h is determined as follows. First, the all-pass nature of h is linearised using the following property: the 2π-periodic frequency response $H(\omega)$ of any digital all-

pass filter can be expressed as

$$H(\omega) = \frac{P\left(\mathrm{e}^{j\omega}\right)}{P\left(\mathrm{e}^{-j\omega}\right)}, \tag{4}$$

where $P\left(\mathrm{e}^{j\omega}\right)$ is the forward and $P\left(\mathrm{e}^{-j\omega}\right)$ the backward version of a real digital filter p. This property allows the all-pass filtering operation performed by h to be expressed linearly as a function of p

$$g_2[k] = h[k] * g_1[k] \iff p[-k] * g_2[k] = p[k] * g_1[k], \tag{5}$$

where $*$ is the convolution operator and k denotes discrete time. Thus, estimating p is equivalent to determining the all-pass filter h however the only constraint on p is that it is real and has a finite impulse response.

The next element is to further reduce the estimation problem by approximating p as a linear combination of a few fixed, known, real filters p_n, i.e.

$$p_{\text{app}}[k] = \sum_{l=0}^{L-1} c_l p_l[k], \tag{6}$$

where L denotes the number of filters and c_l are the coefficients. The estimation of h is thus reduced to determining the L coefficients c_l. In terms of the filter basis, a good choice is a compact, scalable, basis that spans the derivatives of a Gaussian function [13]. For a theoretical foundation on why such a basis is a good choice we refer readers to the analysis presented in [16]. Accordingly, the CLAP algorithm uses the Gaussian function and its first derivatives as a filter basis (i.e. $L = 2$). These filters are defined as

$$p_0[k] = \mathrm{e}^{-k^2/2\sigma^2} \quad \text{and} \quad p_1[k] = k p_0[k], \tag{7}$$

where $\sigma = R/2 - 0.2$ and R is the integer half support of the filters. This parameter R is also the upper bound on the size of the delay the CLAP can estimate.

Putting these elements together, for the local regions exemplified in Fig. 2 the CLAP algorithm solves the following minimisation:

$$\min_{c_1} \sum_{n=1}^{N-1} \sum_{k \in \mathcal{W}} \left| p_{\text{app}}[k] * g_n[k] - p_{\text{app}}[-k] * g_{n+1}[k] \right|^2, \tag{8}$$

where $p_{\text{app}}[k] = p_0[k] + c_1 p_1[k]$ and $\mathcal{W}$ is the local region. The resulting filter obtained from (8) corresponds to the central sample of the local region. By shifting the local region and re-solving (8) to obtain a new all-pass filter and then repeating this process the CLAP estimates a local all-pass filter per sample. Note that as $c_0 = 1$ the minimisation in (8) is equivalent to solving a linear system of equations with 1 unknown, which can be implemented very efficiently using convolution and pointwise multiplication [13]. The last step is to extract the estimate of the TVD signal from the all-pass filters. Using the all-pass structure of the filters, the delay estimate can be expressed in terms of the impulse response p_{app}:

$$\tau_{\text{est}} = 2\frac{\sum_k k p_{\text{app}}[k]}{\sum_k p_{\text{app}}[k]}. \tag{9}$$

The final element in the CLAP algorithm proposed in [12] is an iterative multi-scale framework. The framework allows the CLAP to estimate both fast and slowly varying delays. In brief, although the CLAP is capable of estimating large delays, it requires large filters to do so which is equivalent to assuming large regions of the TVD are slowly varying. Thus, large values of R – the parameter that controls the size of the filter basis – are used initially to estimate large slowly varying components of the TVD, then smaller values of R are used to obtain the faster variations in the TVD. At each iteration, the current estimate of the TVD is used to warp one set of signals closer to the first set and then the update to the delay estimate is determined by solving (8) using filters specified by a smaller value of R.

III. Proposed Approach

In this section we present our method for estimating both the TVD, $\tau(t)$, and the misalignment angle, θ. Our approach is based on the parametric, vector, model of the TVD defined in (2). If we can estimate both $\tau_{\text{col}}(t)$ and $\tau_{\text{row}}(t)$ then we can obtain the misalignment angle by fitting the parametric model to the delay estimates. Once the angle has been determined then the data can be corrected and the actual TVD obtained. Accordingly, our proposed algorithm comprises of two stages. The first stage is to obtain an estimate of the misalignment angle, θ_{est}, via iterative parametric fitting. The second stage is to correct the data using θ_{est} and the estimate the actual TVD by applying the CLAP algorithm on the rotation corrected data.

More specifically, in the first stage, we estimate $\tau_{\text{col}}(t)$ by applying the CLAP algorithm along the columns of the array and estimate $\tau_{\text{row}}(t)$ by applying the CLAP along the rows of the array. Given these delay estimates, the misalignment angle is calculated by computing the mean angle from the TVD vectors defined in (2). This angle estimate is then used to correct the data for the rotation and the process is repeated to refine the estimate of θ. This algorithm is illustrated in Fig. 3. At the ith iteration, the estimate of the misalignment angle is:

$$\theta_i = \theta_{i-1} + \Delta\theta, \tag{10}$$

where $\Delta\theta$ is the circular mean of the TDV vectors:

$$\Delta\theta = \arg\left(\sum_t \tau_{\text{col}}(t) + j\tau_{\text{row}}(t) \right). \tag{11}$$

Note that empirically we have found $K = 4$ to be a good number of iterations to accurately estimate θ.

Moving to the second stage of the algorithm, we apply the CLAP algorithm along the columns of the rotation corrected data to estimate $\tau(t)$. Similar to [12], the single differential of the signals is used in this computation rather than the raw recordings, i.e. $\hat{g}_n(t) = g_{n+1}(t) - g_n(t)$. The reason for this pre-processing step is that in practice sEMG recordings are likely to suffer from common sources of corruption across all of the channels.

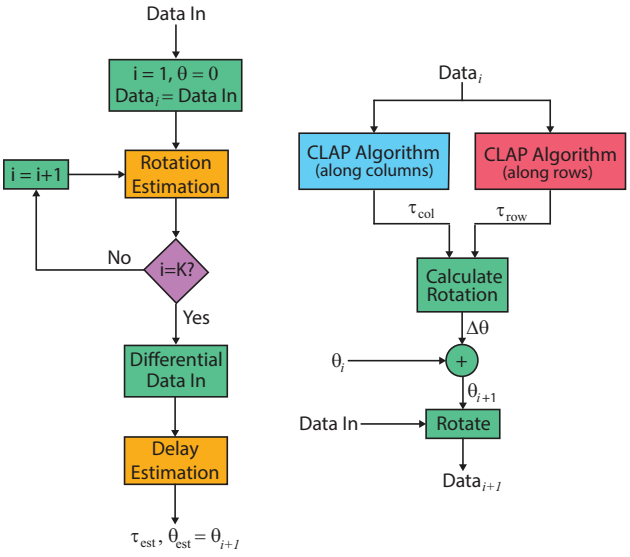

(a) Overall algorithm. (b) Rotation algorithm at each iteration.

Fig. 3. Flowchart of proposed algorithm.

Finally, we end this section with a comment on the rotation operation used to correct the data. The rotation itself is achieved using high quality interpolation detailed in [17], [18]. Depending on the size of the misalignment angle, however, some channels near the top and bottom edges of the array may need to be extrapolated rather than interpolated – the data does not exist for the new position of the electrode after correcting the array for the rotation. This extrapolated data is unreliable and should not be used when estimating the delays along the columns and rows. Accordingly, after the rotation step in Fig. 3b, we determine which electrodes are reliable and use only those in the subsequent CLAP computations.

IV. Synthetic HD-sEMG Model

To simulate realistic sEMG signals a model based on the one proposed in [19] was used. The model as described by Farina and Merletti [19] allows the generation of data from a linear array of electrodes and has been extended for the purposes of this study to a 2D array of electrodes. In brief the model assumes surface electrodes separated from a current density source by a nonhomogeneous, anisotropic volume conductor. The volume conductor is represented as a three layer (nonhomogeneous) medium comprised of muscle tissue (anisotropic), and fat and skin tissues (isotropic). The signal recorded at the skin surface is considered to be the result of both spatial and temporal filtering.

A. Generation of Single Fibre MUAPs

For each individual fibre belonging to a specific MU, the spatial component is modelled by the transfer functions of the volume conductor and of the detection system. With the detection system transfer function taking into account the recording configuration, and the size and shape of the electrodes. The inclination between the fibres and the detection system can be factored in via a rotation of the transfer function of the detection system. The spatial angular frequencies in the x and z directions, that is, perpendicular and parallel to the direction of fibres are $k_x = 2\pi f_x$ and $k_z = 2\pi f_z$, respectively. The output signal, $\varphi(z)$, detected along z (the direction of the fibres) with $x = x_0$ can be computed using a special case of the Radon transform such that

$$\varphi(z) = \Im^{-1}\left\{I(k_z)B(k_z)\right\}, \tag{12}$$

where

$$B(k_z) = \frac{1}{2\pi}\int_{-\infty}^{\infty} H_{glo}(k_x, k_z, \theta)e^{jk_x x_0}dk_x, \tag{13}$$

and $I(k_z)$ is the current density source, $\Im^{-1}$ is the 1D inverse Fourier transform, $H_{glo}(k_x, k_z, \theta) = H_{vc}(k_x, k_z) \cdot H_{ele}(k_x, k_z, \theta)$ and $H_{vc}(k_x, k_z)$ is the transfer function of the volume conductor and $H_{ele}(k_x, k_z, \theta)$ the transfer function of the detection system with rotation θ. For full details of $H_{vc}(k_x, k_z)$ and $H_{ele}(k_x, k_z, \theta)$ we refer the reader to reference [19].

To obtain the signal in time at the location $z = z_0$ the spatial filter $B(k_z)$ given by (13) is applied to the current density source for each instant of time. Which can again be calculated via a special case of the Radon transform such that

$$\varphi(t) = \int_{-\infty}^{\infty}\left(\int_{-\infty}^{\infty} I(k_z, k_t)B(k_z)e^{jk_z k_0}dk_z\right)e^{jk_t t}dk_t \tag{14}$$

where $k_t = 2\pi f_t$ are the temporal angular frequencies and the function $I(k_x, k_t)$ can be computed via the 2D Fourier transform of the current density source. Propagation of the intracellular action potentials (IAPs) cannot just be represented as a shift in time as the current density source needs to account for the effects of the finite fibre length. The model assumes a progressive generation of the first derivative of the IAP at the motor endplate[2] and extinction at the tendons which can be used in conjunction with any mathematical expression of the IAP, for further details we again refer the reader to the detailed description of the model in [19].

B. Generation of sEMG Signals

To generate the sEMG signals which are a summation of the action potentials of many MUs, the recording region of the electrodes was determined according to the method proposed in [20]. The detection volume was defined as the region within the muscle where fibres produce action potentials at the electrode locations which have energy greater than 1/100 of the energy of an action potential of a fibre positioned 1 mm into the muscle directly below the electrodes. To account for the use of a 2D array the width of the recording region was adjusted according to the number of columns in the array, in this case four, and the angle of the array in relation to the

[2]The motor endplate occurs at the neuromuscular junction where the motor neuron innervates the muscle fibre.

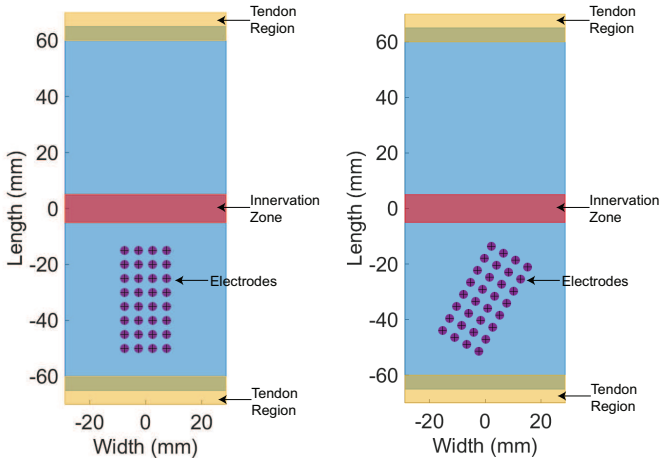

(a) Electrodes inline with fibres. (b) Electrodes at a 30° to fibres.

Fig. 4. Model diagram illustrating the recording configuration for two different electrode placements.

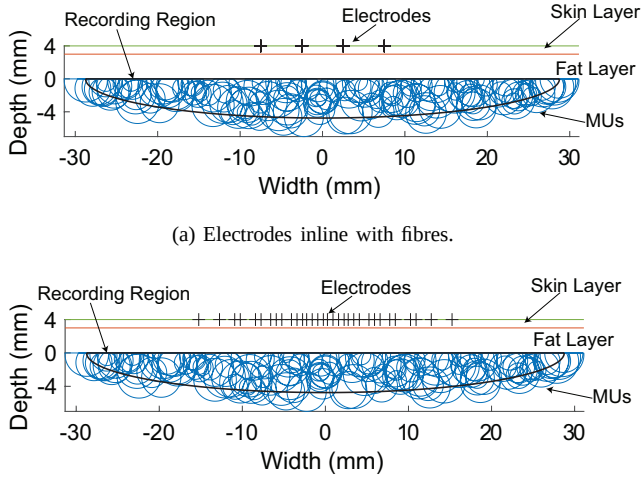

(a) Electrodes inline with fibres.

(b) Electrodes at a 30° to fibres.

Fig. 5. Model diagram illustrating the recording region and motor unit locations for two different electrode placements.

TABLE I
MODEL CONFIGURATION

Parameter		Value
Recording Parameters		
Recording configuration		Monopolar
Array size	Columns Rows	4 8
Electrode shape		Circular
Electrode size	Diameter	3 mm
Interelectrode distance		5 mm
Sampling rate		2 kHz
Recording length		5 sec
Distance centre of array to IZ		-32.5 mm
Angle between array and fibres	Min Max	0° 30°
Muscle Parameters		
IZ spread		10 mm
Tendon region spread	Above IZ Below IZ	10 mm 10 mm
Average semi-fibre lengths	Above IZ Below IZ	65 mm 65 mm
Thickness of fat layer		3 mm
Thickness of skin layer		1 mm
Fibre density	Muscle MU	200 fibres/mm^2 20 fibres/mm^2
Number of motor units		150
Number of fibres per MU	Min Max	50 450
CV distribution	Fixed TV Initial TV Final	4 m/s SD 0.3 m/s 5 m/s SD 0.3 m/s 4 m/s SD 0.7 m/s
CV limits	Min Max	2 m/s 7 m/s
Firing rate		10 Hz SD 15% IPI

IZ - innervation zone; MU - motor unit; CV - conduction velocity; TV - time-varying; SD - standard deviation; IPI - interpulse interval.

fibres, in this case a maximum angle of 30° was used. To allow comparison of the effect of the angle of the array the same width of the recording region was used for all experiments.

The position of the electrode arrays relative to the simulated muscle for angles of 0° and 30° are shown in Fig. 4. An example of the size and location of the different motor units are show in Fig. 5. For each MU the circular cross-sectional area was determined by the number of fibres and the density of the fibres within the MU. The total number of MUs was set to give realistic values of the overall muscle fibre density.

Having obtained the MU sizes and positions, the CV of the MUs were determined according to either a fixed or time-varying scenario. For the fixed scenario the CV were drawn from a Gaussian distribution with a mean of 4 m/s and standard deviation of 0.3 m/s. Whereas for the time-varying scenario the initial distribution had a mean of 5 m/s and a standard deviation of 0.3 m/s and the final distribution a mean of 3 m/s and a standard deviation of 0.7 m/s. In both cases the values of the CVs were truncated to between 2 and 7 m/s to give realistic values. The CVs of the MUs were then sorted according to size with the smallest MUs also having the lowest CV.

The corresponding signals recorded at each of the electrodes were generated based on the combination of the signals from all of the MUs which are in turn the summation of the signals generated by each of the fibres belonging to the MU. A fixed set of 100 realizations of the MU sizes and positions were used for all of the simulations and the MUAPs were calculated as in Section IV-A for each of the angle and CV scenarios. The signals were generated using fixed firing rate for all of the MUs. All of the model parameters used in the simulations are summarized in Table I.

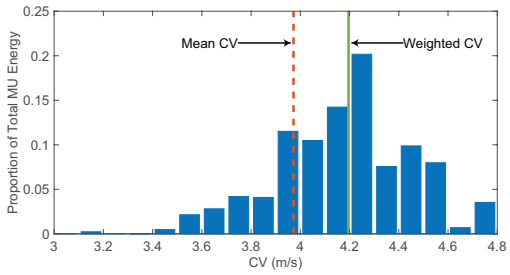

Fig. 6. An example of the distribution of the contribution of the motor unit energies to the conduction velocity.

V. Simulations

A. Ensemble MFCV

Before estimating the MFCVs we needed to consider how the superposition of the MUs affects the MFCV observed at the electrodes. Although the CVs of each MU were drawn from a Gaussian distribution the MFCV measured from the sEMG does not directly correspond to this distribution. As smaller MUs have slower CVs and larger MUs faster CVs the distribution of the MFCV becomes skewed towards the faster CVs. At the same time the location of MUs within the recording region affects how great a contribution they make to the overall sEMG signal. To provide an estimate of the overall ensemble MFCV as observed at the surface of the skin we calculated the energy of the signals produced by each MU across all of the electrodes. The contributions of the CVs of each MU were then calculated by weighting the CV according to the proportion of the total energy of all of the MUs the MU provides, such that the weighted CV, wCV is given by

$$wCV = CV_1\frac{e_1}{E} + CV_2\frac{e_2}{E} + \ldots + CV_{150}\frac{e_{150}}{E}, \quad (15)$$

where

$$E = \sum_{i=1}^{150} e_i, \quad (16)$$

and e_i is the energy of the signals produced by MU i and CV_i the corresponding CV. Figure 6 illustrates the contributions of the MU energies for different CVs as a proportion of the total MU energy. As can be seen this distribution is no longer Gaussian and the weighted CV gives a more accurate representation of the distribution of the energies than the mean CV. Therefore, the weighted CV was used in the subsequent analysis as a ground truth measure of the ensemble MFCV against which to compare the estimates obtained from the CLAP.

B. Accuracy of Ensemble MFCV Estimation

Using the measure of the ensemble MFCV as recorded by the sEMG described above we then calculated the mean absolute error (MAE) between the ensemble MFCV and the estimates of the fixed CV obtained from the CLAP algorithm. Figure 7a shows the average MAE obtained from 100 realizations for misalignment angles upto 30°. The results

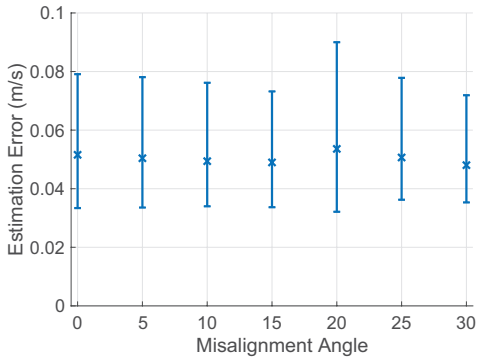

(a) Error in the estimates of the fixed MFCV.

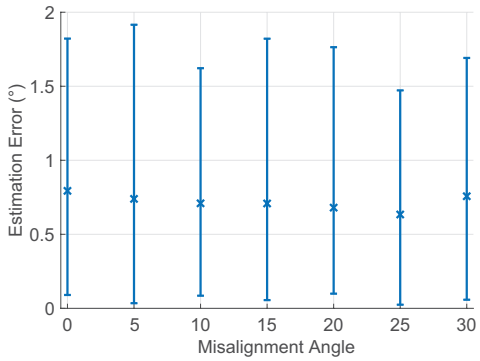

(b) Error in the estimates of the misalignment angle.

Fig. 7. Average errors for increasing misalignment angles with fixed CV. Error bars indicate 5^{th} and 95^{th} quantiles.

demonstrate that estimates were not only accurate and robust but also the errors were relatively consistent across the different misalingnment angles. The corresponding estimates of the misalignment angles are shown in Fig. 7b, again the average MAE was consistent across angles with the results indicating 95% of the estimates have an error of less than 2 degrees.

For the method to be applicable in a wider range of scenarios it must also be capable of solving the TVD problem in the context of misalignment of the electrode array. Figure 8a gives an example of the distribution of the time-varying CVs from one of the set of MUs used to test our proposed approach. As well as the mean and standard deviation of the distribution, the range of the CVs are displayed along with the weighted CV. Figure 8b shows the estimate of the ensemble MFCV obtained using the CLAP algorithm, as can be seen the estimate accurately tracks the time-varying MFCV with a MAE of 0.06 m/s. The distribution of the MAEs for the time-varying CVs are shown in Fig. 9. The average errors are again consistent across the range of misalignment angles although with slightly higher values than for the fixed MFCV. As with the estimates of the MFCV, the estimates of the misalignment angle are consistent across the angles with average errors of less than one degree.

VI. Conclusions

The requirement to accurately place electrodes whilst setting up for sEMG recordings is a limitation if it is to be used in

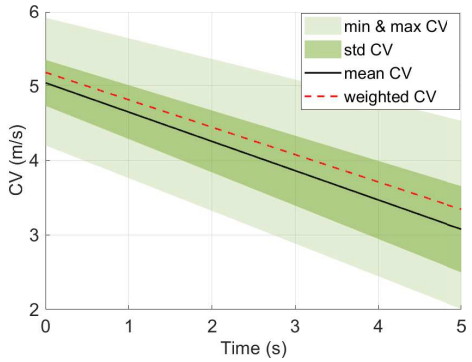

(a) CV Distribution.

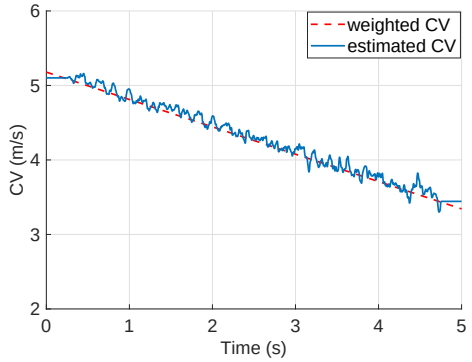

(b) Estimated MFCV.

Fig. 8. An example of the distribution of the MU CVs for one realization and the corresponding MFCV estimate obtained from the CLAP algorithm.

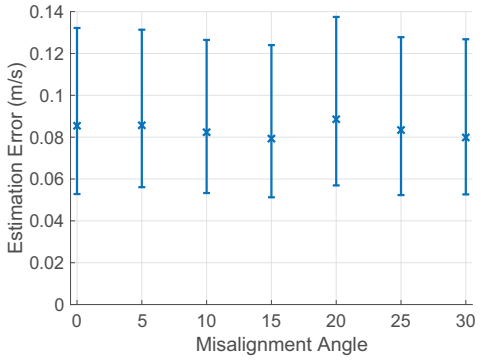

(a) Error in the estimates of time-varying MFCV.

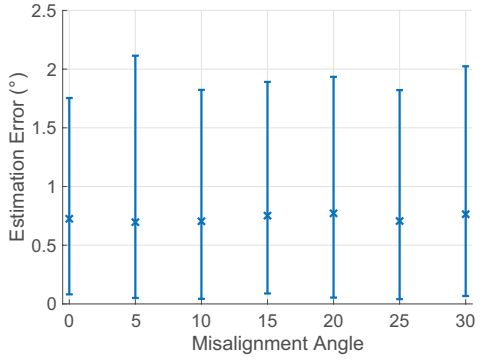

(b) Error in the estimates of the misalignment angle.

Fig. 9. Average errors for increasing misalignment angle with time-varying CV. Error bars indicate 5^{th} and 95^{th} quantiles.

a wider range of scenarios. In this paper, we have presented an extension of our earlier work which estimates TVDs for the purposes of calculating MFCV. Here we take into account the effect of misalignment between the muscle fibres and the electrode array on the delay estimation. By modelling the misalignment as a rotation of the array and iteratively fitting we can estimate the misalignment angle and hence, improve the TVD estimation. Results show that the proposed method accurately estimates both the misalignment angle and the true delay in the direction of the fibres. However, we feel these results can be improved further by applying parametric iterative fitting as described in [21] to the delay estimation. Our approach provides a more practical solution to MFCV estimation which allows accurate estimates without the need for perfect alignment of the array with the muscle fibre.

REFERENCES

[1] M. Hakonen, H. Piitulainen, and A. Visala, "Current state of digital signal processing in myoelectric interfaces and related applications," *Biomedical Signal Processing and Control*, vol. 18, pp. 334–359, 2015.

[2] R. A. Sherman, "Instrumentation methodology for recording and feeding-back surface electromyographic (SEMG) signals," *Appl. Psychophysiol. Biofeedback*, vol. 28, no. 2, pp. 107–119, 2003.

[3] H. J. Hermens, B. Freriks, C. Disselhorst-Klug, and G. Rau, "Development of recommendations for SEMG sensors and sensor placement procedures," *J. Electromyogr. Kinesiol.*, vol. 10, no. 5, pp. 361–374, 2000.

[4] R. Chowdhury, M. Reaz, M. Ali, A. Bakar, K. Chellappan, and T. Chang, "Surface electromyography signal processing and classification techniques," *Sensors*, vol. 13, no. 9, pp. 12431–12466, 2013.

[5] M. J. Zwarts, G. Drost, and D. F. Stegeman, "Recent progress in the diagnostic use of surface EMG for neurological diseases," *J. Electromyogr. Kinesiol.*, vol. 10, no. 5, pp. 287–291, 2000.

[6] D. Farina and R. Merletti, "Estimation of average muscle fiber conduction velocity from two-dimensional surface EMG recordings," *J. Neurosci. Methods*, vol. 134, no. 2, pp. 199–208, 2004.

[7] E. Schulte, O. Miltner, E. Junker, G. Rau, and C. Disselhorst-Klug, "Upper trapezius muscle conduction velocity during fatigue in subjects with and without work-related muscular disorders: a non-invasive high spatial resolution approach," *Eur. J. Appl. Physiol.*, vol. 96, no. 2, pp. 194–202, 2006.

[8] C. Grönlund, N. Östlund, K. Roeleveld, and J. S. Karlsson, "Simultaneous estimation of muscle fibre conduction velocity and muscle fibre orientation using 2D multichannel surface electromyogram," *Med. Biol. Eng. Comput.*, vol. 43, no. 1, pp. 63–70, 2005.

[9] A. Boualem, M. Jabloun, P. Ravier, and O. Buttelli, "Legendre polynomial modeling of time-varying delay applied to surface EMG signals — derivation of the appropriate time-dependent CRBs," *Signal Process.*, vol. 114, pp. 34–44, 2015.

[10] P. Ravier, D. Farina, and O. Buttelli, "Time-varying delay estimators for measuring muscle fiber conduction velocity from the surface electromyogram," *Biomed. Signal Process. Control*, vol. 22, pp. 126–134, 2015.

[11] S. H. Roy, C. J. De Luca, and J. Schneider, "Effects of electrode location on myoelectric conduction velocity and median frequency estimates.," *J. Appl. Physiol.*, vol. 61, pp. 1510–1517, 1986.

[12] C. Gilliam, A. Bingham, T. Blu, and B. Jelfs, "Time-varying delay estimation using common local all-pass fitlers with application to surface electromyography," in *Proc. IEEE Int. Conf. on Acoustics, Speech and Signal Processing (ICASSP)*, Calgary, Canada, 2018, pp. 841–845.

[13] C. Gilliam and T. Blu, "Local all-pass geometric deformations," *IEEE Trans. Image Process.*, vol. 27, no. 2, pp. 1010–1025, 2018.

[14] C. Gilliam, T. Küstner, and T. Blu, "3D motion flow estimation using local all-pass filters," in *Proc. IEEE Int. Symp. on Biomedical Imaging (ISBI)*, Prague, Czech Republic, 2016, pp. 282–285.

[15] J. Li, C. Gilliam, and T. Blu, "A multi-frame optical flow spot tracker," in *Proc. IEEE Int. Conf. on Image Processing (ICIP)*, Québec City, Canada, 2015, pp. 3670–3674.

[16] T. Blu, P. Moulin, and C. Gilliam, "Approximation order of the LAP optical flow algorithm," in *Proc. IEEE Int. Conf. on Image Processing (ICIP)*, Québec City, Canada, 2015, pp. 48–52.
[17] P. Thévenaz, T. Blu, and M. Unser, "Interpolation revisited," *IEEE Trans. Med. Imag.*, vol. 19, no. 7, pp. 739–758, 2000.
[18] T. Blu, P. Thévenaz, and M. Unser, "MOMS: Maximal-order interpolation of minimal support," *IEEE Trans. Image Process.*, vol. 10, no. 7, pp. 1069–1080, 2001.
[19] D. Farina and R. Merletti, "A novel approach for precise simulation of the EMG signal detected by surface electrodes," *IEEE Trans. Biomed. Eng.*, vol. 48, no. 6, pp. 637–646, 2001.
[20] D. Farina, M. Fosci, and R. Merletti, "Motor unit recruitment strategies investigated by surface EMG variables," *J. Appl. Physiol.*, vol. 92, no. 1, pp. 235–247, 2002.
[21] X. Zhang, C. Gilliam, and T. Blu, "Iterative fitting after elastic registration: An efficient strategy for accurate estimation of parametric deformations," in *Proc. IEEE Int. Conf. on Image Processing (ICIP)*, Beijing, China, 2017, pp. 1492–1496.